ACS OMEGA

Open Access

http://pubs.acs.org/journal/acsodf

Article

Integrated Humin Formation and Separation Studied In Situ by Centrifugation

Alexander Walter Wilhelm Echtermeyer and Jörn Viell*

Cite This: *ACS Omega* 2024, 9, 6432−6441

Read Online

ACCESS | Metrics & More | Article Recommendations | Supporting Information

ABSTRACT: We present a novel method for studying the integrated formation and separation of humins formed during the Brønsted acid-catalyzed conversion of fructose (here, at 90 °C with 20 wt % fructose and 5 wt % sulfuric acid). For the first time, we report the reaction carried out in situ during systematic centrifugation experiments, which allows combining humin formation and separation along with investigation of the phase behavior of humins. Analysis of the formed humin deposits employing scanning electron microscopy reveals deposits that are formed from a layer of monodisperse microspheres with a narrow diameter range of 0.9−1.9 μm. In the centrifugal force field, the microspheres partially coalesce, which increases with time and relative centrifugal force up to the formation of a thin and uniform layer of microspheres covering a continuous humin bulk phase with 80−90 μm thickness. These findings give evidence that humin spheres are highly viscous droplets rather than solid particles during formation. Our result is in line with the often-reported spherical and planar deposits formed during acidic carbohydrate conversion in technical systems and supports the development of strategies for deposit prevention, on the one hand, and humin preparation for material utilization, on the other hand.

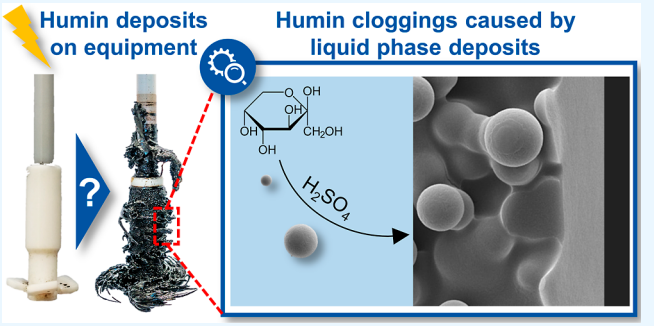

1. INTRODUCTION

The Brønsted acid-catalyzed conversion of carbohydrates such as lignocellulosic biomass and thereof derived monosaccharides is impaired by side reactions forming tar-like residues, generally termed humins.[1,2] Arising from random cross-polymerizing condensation reactions of intermediates that are unstable under acidic conditions, humins can cause diminished process yield and a carbon loss of up to 50%.[3−8] Moreover, humins lead to severe deposit formation in reactors and pipelines and on sensors that detrimentally impact heat transfer, flow conditions, and process analytics.[1,9] Given the results of extensive kinetic studies, the formation of humin side products is inevitably coupled to the monosaccharide reaction and cannot be suppressed thermodynamically.[10−16] Recent reviews identify the intermediate 5-hydroxymethylfurfural (5-HMF) as a core molecule of carbohydrate conversion reactions and also the main precursor of humins. A comprehensive overview of reaction mechanisms, scientific progress, and remaining challenges to minimize the formation of undesired humin side products is given in literature.[17,18] Both reviews show that with careful catalyst selection and the use of additives such as organic solvents in mono- and multiphase operation, humin formation can be reduced but only at the expense of process complexity and increased costs. Hence, understanding the mesoscale mechanism for humin formation and deposition in comparatively simple and low-cost reaction environments supports knowledge-based improvement of operating conditions and the design of technical systems in order to prevent such deposits.

To reduce the complexity of the reaction network from various sugars, the conversion of fructose (FRC) with side reactions to humin has been studied in detail.[5,13,19,20] After separation from the reaction mixture, the formed humins have been characterized as solid carbon microspheres with variable morphology and diameter depending on time, temperature, feedstock concentration, and additives.[6,14,19−23] Accordingly, solid-based formation mechanisms are assumed in most studies.[8,22−26] However, some recent research gives evidence that humin spheres form as highly viscous liquid droplets instead of solid particles because the growth of the spheres is recognized after feedstock depletion, indicating coagulation, and a strongly altered humin shape due to shearing by stirring of the reaction mixture is observed.[21,27] Clearly, the spherical morphology of some particles indicates the presence of a liquid state during formation, but it has been neither observed systematically nor formulated as a complete hypothesis of

Received: August 17, 2023
Revised: November 30, 2023
Accepted: January 9, 2024
Published: January 31, 2024

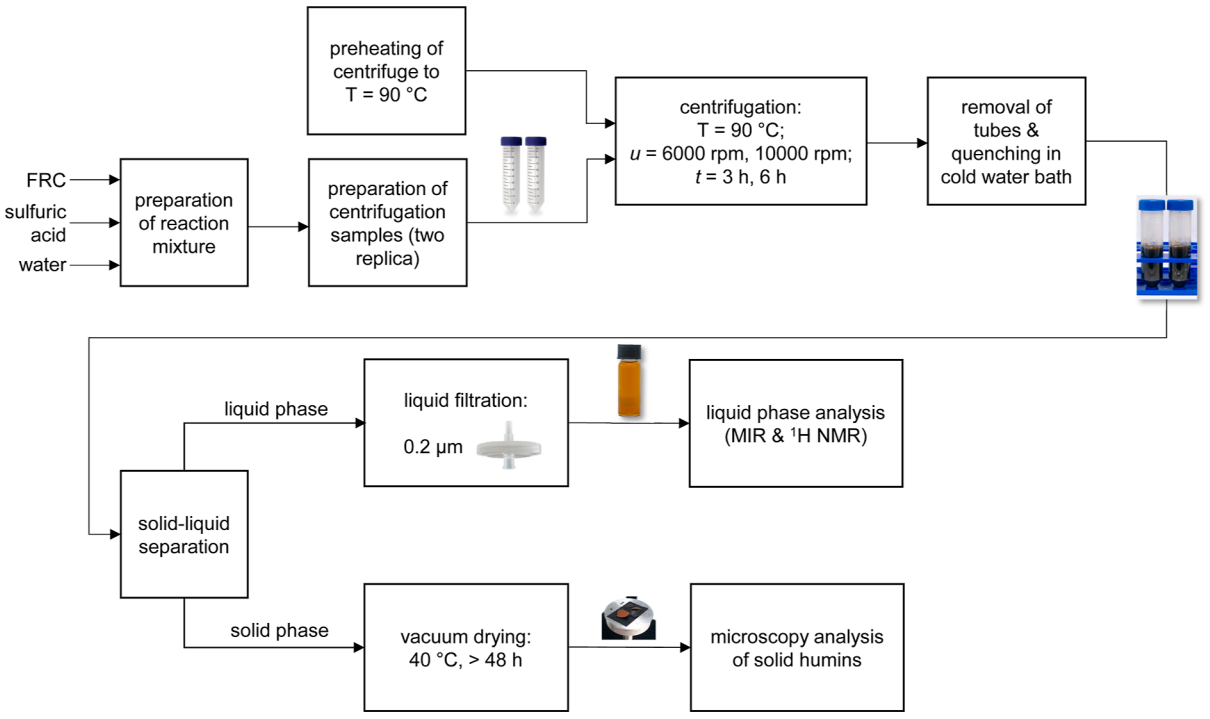

Figure 1. Schematic representation of the experimental procedure from reaction mixture preparation to sample analysis (FRC: fructose, MIR: mid-infrared, NMR: nuclear magnetic resonance).

humin formation as highly viscous droplets up to the formation of solid layers of deposits. Based on the reported assumption that liquid humin droplets could be altered in morphology by shearing such as at stirred reaction conditions, we additionally hypothesize that liquid humin droplets could be forced into coalescence by application of a strong gravitational field.[27] In this contribution, we present a method based on centrifugation to study the formation and separation of humin material in view of the mesoscale mechanism of humin formation, along with a selective in situ humin separation for potential subsequent humin utilization. Based on our results, we consolidate the concept of humin spheres as highly viscous droplets during formation by reporting systematic centrifugation experiments under process conditions.

2. METHODS

2.1. Experimental Procedure. A process scheme for the centrifugation experiments is provided in Figure 1.

Samples containing 20 wt % FRC (VWR International GmbH, ≥99%), 5 wt % sulfuric acid (VWR International GmbH, ≥98%), and a remainder of deionized water (produced in-house, conductivity ≤0.8 μS cm^{-1} at 25 °C) are prepared by first mixing water and sulfuric acid with subsequent addition of the corresponding amount of FRC. Two identical samples per reaction condition are prepared by filling each 25 g of the mixture in 50 mL polypropylene centrifugal tubes (Thermo Fisher Scientific Inc.). The centrifugal tubes are placed in a centrifuge (ROTINA 420, Hettich GmbH + Co. KG) that is preheated to the reaction temperature of 90 °C (temperature limit for the centrifuge). The centrifuge is adjusted to 6000 and 10,000 rpm, which translates into a relative centrifugal force (RCF) of 4790 and 13,304, respectively. After a reaction time t of 3 h in case of 6000 and 10,000 rpm and for 6 h in case of 10,000 rpm, the centrifuge is stopped and the reaction is terminated by carefully quenching the centrifugal tubes in cold water. While about 4 mL of the liquid supernatant is secured and filtered (0.2 μm nylon syringe filter, VWR International GmbH) for subsequent liquid-phase analysis, the remainder is carefully disposed of without disturbing the humin residues at the wall of the centrifugal tubes. Thereupon, the centrifugal tubes with deposited humin residues are dried under vacuum at 40 °C for at least 48 h and are subsequently subjected to humin deposit analysis. For reference, the reaction is executed in a heating block (no stirring) without a centrifuge at an RCF of 1 for 6 h, and the obtained material is treated as outlined above. Images are taken of the liquid supernatant and centrifugal tubes for visual comparison (see Figure S9 in the Supporting Information).

2.2. Analytics. *2.2.1. Microscopy of Humin Deposits.* The humin deposits are analyzed employing a benchtop scanning electron microscope of type TM3030Plus and an analytical field emission (FE) scanning electron microscope of type SU5000, both from Hitachi Ltd. Scanning electron microscopy (SEM) images are taken at 15 kV with large current mode and recording of backscattered and secondary electrons (mixed observation) with charge-up reduction function. Figures S6 and S7 in the Supporting Information depict the sample preparation for the acquisition of SEM images. FESEM images are collected after gold−palladium sputtering of the samples at 5 kV and recording of the secondary electrons.

To determine the size distribution of the formed humin spheres, 30 spheres are measured in the SEM and FESEM images of the solid material obtained from each investigated reaction condition, as indicated by black numbers in Figure S10 in the Supporting Information. Spherical subunits were measured in the case of merged structures with recognizable spherical shapes.

2.2.2. Spectroscopy for the Liquid Phase. In a long-term perspective, real-time process monitoring of Brønsted acid-catalyzed conversion of carbohydrates is envisioned.[17,18] To set

https://doi.org/10.1021/acsomega.3c06103
ACS Omega 2024, 9, 6432−6441

the basis for this goal in the present work, two process spectroscopy methods, fiber-optical mid-infrared (MIR) and benchtop ^{1}H nuclear magnetic resonance (NMR) spectroscopy, are employed for the determination of the liquid-phase composition.

MIR spectra are recorded using a Matrix-MF$^+$ Fourier transform MIR spectrometer (Bruker Optics GmbH) coupled with a fiber-optic IN350-T diamond attenuated total reflection immersion probe (Bruker Optics GmbH). The system is cooled with liquid nitrogen and conditioned with dry air. MIR spectra are recorded in absorbance mode with OPUS ver. 7.5 (Bruker Optics GmbH) setting a resolution of 4 cm^{-1} and 100 scans per spectrum in a total spectral range of $\tilde{\nu}$ = 700−4000 cm^{-1}. Prior to each sample measurement, the diamond probe tip is carefully cleaned with acetone and compressed air followed by the acquisition of a background spectrum in deionized water.

For comparison, the liquid phase is measured by ^{1}H NMR spectroscopy. Prior to the ^{1}H NMR measurement, liquid samples are prepared by thoroughly mixing defined sample masses with defined masses of *tert*-butanol (Merck KGaA, ≥99.5%) as an internal standard in 4 mL vials followed by transfer into NMR tubes for ^{1}H NMR measurement. ^{1}H NMR spectra are recorded by employing a benchtop NMR spectrometer of the type Spinsolve Carbon operating at 42.5 MHz with flow-through feasibility (Magritek GmbH). ^{1}H NMR spectra are collected using the software Spinsolve ver. 1.19.0 (Magritek GmbH) with the standard settings of the 1D Proton protocol (40 scans per spectrum with 6.6 s acquisition time, 15 s repetition time, and 90° excitation pulse). Postprocessing of the ^{1}H NMR spectra in the software MestReNova ver. 14.1.0 (Mestrelab Research S.L.) comprises linear baseline correction and phase adjustment (PH0 = 1, PH1 = 0) as well as referencing of the *tert*-butanol peak position to 1.254 ppm.

2.3. Chemometric Models. *2.3.1. Visual Analysis and Pretreatment of Spectral Data.* Visual analysis and pretreatment of the MIR and ^{1}H NMR spectra are performed in the software PEAXACT ver. 5.8 (S-PACT GmbH).[28] In the case of MIR spectra, a spectral range of $\tilde{\nu}$ = 800−1800 cm^{-1} is evaluated, whereas in the case of ^{1}H NMR spectra, a spectral range of 0−10 ppm with the exclusion of the strong signals from water protons in the range of 4.5−5.5 ppm is selected. For both MIR and ^{1}H NMR spectra, a linear fit baseline is subtracted, and neither standardization methods nor derivatives and data smoothing are applied.

2.3.2. Indirect Hard Modeling. The recorded MIR and ^{1}H NMR spectra are translated into quantitative composition information by employing two chemometric models. Both models are based on spectral complemental hard modeling and spectral indirect hard modeling.[29−31] They are constructed, calibrated, validated, and applied by using the software PEAXACT in each step.

With the first chemometric or spectral mixture hard model, MIR spectra are quantitatively evaluated for mass fractions of FRC, 5-HMF, levulinic acid (LA), formic acid (FA), sulfuric acid, and water, whereas with the second spectral mixture hard model, ^{1}H NMR spectra are quantified for FRC, 5-HMF, LA, and FA, respectively.

Details on the construction of both spectral mixture hard models together with further information on the theoretical concept of spectral complemental hard modeling and spectral indirect hard modeling are provided in the Supporting Information. The advantages of spectral indirect hard modeling over other multivariate chemometric models, such as often-used partial least squares regression, are the physically meaningful deconvolution of highly overlapping peaks in the spectra of multicomponent mixtures, the compensation of nonlinear effects such as peak shifts or peak deformations due to the interaction of chemical species, the robustness against noise,[29,32] a reduced demand of calibration samples,[29,33] and the improved range of extrapolation, e.g., in composition and temperature dimension[29,34] that have been reported in the literature and are mostly explained by the physically motivated structure of the spectral indirect hard modeling.

2.3.3. Calibration and Validation of Chemometric Models. For calibration of the MIR spectral mixture hard model, a total number of 201 MIR mixture spectra with corresponding composition data in terms of mass fractions w_k with $k \in$ {FRC, LA, FA, 5-HMF, and sulfuric acid} are employed. The ^{1}H NMR spectral mixture hard model is calibrated by employing a total number of 236 ^{1}H NMR mixture spectra with corresponding composition data in terms of mass fractions w_k with $k \in$ {FRC, LA, FA, and 5-HMF}.

For both MIR and ^{1}H NMR spectral mixture hard models, leave-10%-out cross-validations are executed during calibration. The quality of the spectral mixture hard model calibrations with regard to each chemical species k is assessed by the coefficient of determination and the root mean square error of cross-validation. Furthermore, both calibrated spectral mixture hard models are employed in an external validation by analyzing 82 defined samples for MIR spectroscopy and 32 defined samples for ^{1}H NMR spectroscopy to obtain values for the root mean square error of prediction of both spectral mixture hard models, respectively. Finally, the limit of detection based on 10 blank MIR and ^{1}H NMR measurements of deionized water, respectively, is determined for both spectral mixture hard models.

For further details on the calibration, validation, and calculation of the respective figures of merit, please refer to the Supporting Information.

2.4. Mass Balance Calculation. According to a recent study of humin growth kinetics during the HCl-catalyzed dehydration of FRC, humin is predominantly formed from 5-HMF rather than from FRC.[22] Hence, together with the assumption of 5-HMF as the only species forming humin during the dehydration of FRC and the reaction scheme displayed in Figure S8, a mass balance for the FRC-based reaction is derived in eq 1 (please refer to Figure S8 for further explanation)

$$0 \overset{!}{=} m_{\mathrm{FRC},0} - m_{\mathrm{FRC}} - m_{\mathrm{5-HMF}} - m_{\mathrm{LA}} - m_{\mathrm{FA}} - m_{\mathrm{humin}} - M_{\mathrm{H_2O}}\left(4\frac{m_{\mathrm{FRC},0} - m_{\mathrm{FRC}}}{M_{\mathrm{FRC}}} - 3\frac{m_{\mathrm{LA}}}{M_{\mathrm{LA}}} - \frac{m_{\mathrm{5-HMF}}}{M_{\mathrm{5-HMF}}}\right) \quad (1)$$

The difference between the initial mass of FRC ($m_{\mathrm{FRC},0}$) at the beginning of the reaction (reaction time t = 0) and the mass of remaining FRC m_{FRC} together with the masses of the reaction products m_k and molar masses M_k with $k \in$ {FRC, LA, FA, 5-HMF, and humin} in the course of the reaction ($t > 0$) is zero for a closed mass balance. In eq 1, the consumption and formation of water during the overall reaction are likewise considered.[13,22] We account for the dehydration of FRC to 5-HMF with the formation of 3 mol of water per mole of formed

https://doi.org/10.1021/acsomega.3c06103
ACS Omega 2024, 9, 6432−6441

Table 1. Results of Centrifugation Experiments in Terms of Species Mass Fractions w_k with $k \in$ {FRC, 5-HMF, FA, LA, Sulfuric Acid, and Humin} at Different RCF and Reaction Times t of 3 and 6 h[a]

		t = 3 h		t = 6 h	
variable	unit	RCF = 4790	RCF = 13,304	RCF = 1	RCF = 13,304
w_{FRC}	wt %	15.3 ± 0.50	14.7 ± 0.13	6.8 ± 0.86	10.1 ± 0.39
$w_{5\text{-HMF}}$	wt %	1.8 ± 0.09	2.1 ± 0.02	2.8 ± 0.23	2.5 ± 0.38
w_{FA}	wt %	0.4 ± 0.19	0.6 ± 0.36	1.6 ± 0.16	1.1 ± 0.33
w_{LA}	wt %	0.5 ± 0.04	0.4 ± 0.36	3.5 ± 0.31	2.0 ± 0.15
$w_{\text{sulfuric acid}}$[b]	wt %	6.3 ± 0.01	6.0 ± 0.03	6.2 ± 0.08	6.1 ± 0.07
w_{humin}	wt %	0.7 ± 0.16	0.6 ± 0.28	1.9 ± 0.26	1.8 ± 0.98

[a]All values except mass fractions for sulfuric acid are based on two identical samples per reaction condition and averaged results for MIR and ^{1}H NMR analytics. [b]Mass fractions based on two identical samples per reaction condition but only from MIR analytics as sulfuric acid is not directly detected with ^{1}H NMR spectroscopy.

5-HMF. The rehydration of 5-HMF to LA and FA consumes 2 mol of water per mole of formed LA. The condensation of 5-HMF to humin forms 1 mol of water per mole of condensed 5-HMF following an approach reported by Jung et int. Kruse.[21]

Only the liquid phase is analyzed by ^{1}H NMR and MIR spectroscopy after cooling and filtration of the reaction sample. Therefore, the corresponding liquid mass as the difference of the total mass from sample preparation $m_{tot,0}$ and the mass of the formed and at ambient conditions solid humin species m_{humin} has to be considered as a basis for the liquid-phase mass balance.

$$m_{FRC,0} = w_{FRC,0} m_{tot,0} \tag{2}$$

While the mass of FRC at $t = 0$ is known from sample preparation according to eq 2, the masses of all other species m_k after a certain reaction time $t > 0$ are calculated using mass fraction data w_k with $k \in$ {FRC, LA, FA, and 5-HMF} from spectroscopic analysis of the liquid sample in eq 3

$$m_k = w_k (m_{tot,0} - m_{humin}) \tag{3}$$

The mass of formed humin (m_{humin}) can be expressed as the mass fraction of humin (w_{humin}) on the basis of the overall reaction mass $m_{tot,0}$ following eq 4

$$m_{humin} = w_{humin} m_{tot,0} \tag{4}$$

Please refer to Figure S8 for further explanatory visualization.

Given a closed mass balance, eqs 1−4 can be reorganized to yield the mass fraction of formed humin (w_{humin}) solely from spectroscopy results and sample preparation data as input at a reaction time $t > 0$ by eq 5

$$w_{humin} = \frac{w_{FRC,0} - w_{FRC} - w_{5-HMF} - w_{LA} - w_{FA} - M_{H_2O}\left(4\frac{w_{FRC,0} - w_{FRC}}{M_{FRC}} - 3\frac{w_{LA}}{M_{LA}} - \frac{w_{5-HMF}}{M_{5-HMF}}\right)}{1 - w_{FRC} - w_{5-HMF} - w_{LA} - w_{FA} + M_{H_2O}\left(4\frac{w_{FRC,0} - w_{FRC}}{M_{FRC}} + 3\frac{w_{LA}}{M_{LA}} + \frac{w_{5-HMF}}{M_{5-HMF}}\right)} \tag{5}$$

Here, M_k denotes the molar masses of the species and $w_{FRC,0}$ represents the initial mass fraction of FRC at the start of the reaction.

2.5. Stoichiometric Figures of Merit. The molar yield of humin (Y_{humin}) is calculated subject to eq 6 with M_{humin} = 108.1 g mol^{-1} as the molar mass of humin.[13,21]

$$Y_{humin} = \frac{(w_{humin} - w_{humin,0})}{w_{FRC,0}} \frac{M_{FRC}}{M_{humin}} \times 100 \text{ mol \%} \tag{6}$$

Under consideration of a reduced overall liquid sample mass in the course of the reaction ($t > 0$) compared to the initial liquid sample mass ($t = 0$) due to humin formation (cf. eq 3), the molar yields Y_k of the remaining species k with $k \in$ {LA, FA, and 5-HMF} are calculated subject to eq 7

$$Y_k = \frac{(w_k - w_{k,0})(m_{tot,0} - m_{humin})}{m_{FRC,0}} \frac{M_{FRC}}{M_k} \times 100 \text{ mol \%} \tag{7}$$

which is reformulated using eqs 2−4, resulting in eq 8

$$Y_k = \frac{(w_k - w_{k,0})(1 - w_{humin})}{w_{FRC,0}} \frac{M_{FRC}}{M_k} \times 100 \text{ mol \%} \tag{8}$$

By consideration of the reduced liquid sample mass during the reaction similar to eqs 7 and 8, the conversion of FRC (X_{FRC}) is calculated subject to eq 9

$$X_{FRC} = \frac{w_{FRC,0} - w_{FRC}(1 - w_{humin})}{w_{FRC,0}} \times 100 \text{ wt \%} \tag{9}$$

3. RESULTS AND DISCUSSION

In the following section, the results of the centrifugation experiments in terms of the liquid-phase and solid-phase investigations are analyzed and discussed. The analysis is based on the results of the chemometric models used for the liquid-phase-composition determination. As chemometric model development, calibration, and validation were satisfying according to the standard figures of merit for quality judgment, further details are not discussed in the main article but are comprehensively provided in the Supporting Information, Section S3.

The acid-catalyzed reaction of 20 wt % FRC at 5 wt % sulfuric acid in aqueous solution has been set up to resemble the high-solid, acid-catalyzed conversion of lignocellulosic biomass in a lignocellulosic biorefinery.[16,35,36] Moreover, the conditions are chosen to produce significant amounts of humins at the reaction temperature of 90 °C in the centrifuge

https://doi.org/10.1021/acsomega.3c06103
ACS Omega 2024, 9, 6432−6441

Table 2. Results of Centrifugation Experiments in Terms of FRC Conversion X_{FRC} and Species Yield Y_k with $k \in$ {5-HMF, FA, LA, and Humin} at Different RCF and Reaction Times t of 3 and 6 h[a]

		t = 3 h		t = 6 h	
variable	unit	RCF = 4790	RCF = 13,304	RCF = 1	RCF = 13,304
X_{FRC}	wt %	23.8 ± 2.54	26.9 ± 0.86	66.1 ± 4.35	50.3 ± 2.38
$Y_{5\text{-HMF}}$	mol %	12.6 ± 0.64	14.7 ± 0.15	20 ± 1.66	17.5 ± 2.82
Y_{FA}	mol %	8.9 ± 3.07	12.4 ± 6.97	48.8 ± 16.84	29.7 ± 9.37
Y_{LA}	mol %	4.2 ± 0.30	3.2 ± 2.78	27.1 ± 2.73	15.5 ± 1.20
Y_{humin}	mol %	6.0 ± 1.31	5.2 ± 2.36	16.6 ± 2.18	15.2 ± 8.12

[a]All values are based on two identical samples per reaction condition and averaged results for MIR and ^{1}H NMR analytics.

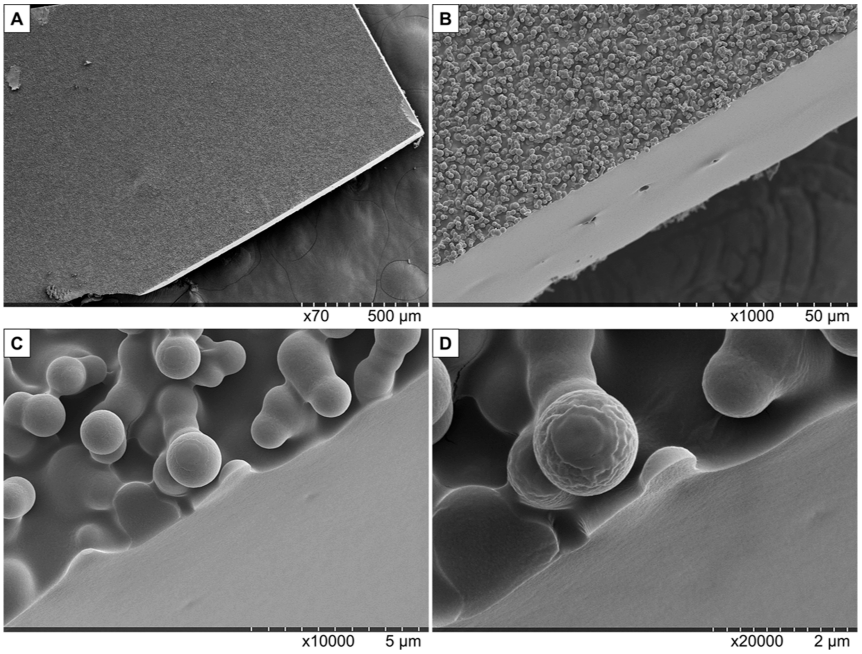

Figure 2. FESEM images of humin deposits from the wall of the centrifugal tube at different magnifications for the centrifugation experiment converting 20 wt % FRC in an aqueous solution of 5 wt % sulfuric acid at 90 °C and an RCF of 13,304 for 6 h. The images indicate the thin, almost monodisperse layer of humin spheres (A, B) covering and partially merging a continuous, planar humin bulk phase (C, D).

Table 3. Results of Centrifugation Experiments in Terms of Minimum Diameter (d_{min}), Maximum Diameter (d_{max}), and Average Diameter (d_{avg}) with Standard Deviation for 30 Humin Spheres Measured per Experiment from Corresponding SEM and FESEM Images at Different RCF and Reaction Times t of 3 and 6 h (cf. Figure S10)

	unit	t = 3 h		t = 6 h	
variable		RCF = 4790	RCF = 13,304	RCF = 1	RCF = 13,304
d_{min}	µm	1.1	1.4	2.6	0.9
d_{max}	µm	3.6	2.6	14.0	1.9
d_{avg}	µm	2.3 ± 0.6	2.1 ± 0.2	6.7 ± 2.6	1.3 ± 0.3

using sulfuric acid as a catalyst.[8] The mass fractions of the analyzed chemical species under the respective reaction conditions are stated in Table 1. The associated stoichiometric figures of merit, such as the conversion of FRC and yields of the products under the investigated reaction conditions, are provided in Table 2. At an RCF of 13,304 for 6 h, an FRC mass fraction of w_{FRC} = 10.1 ± 0.39 wt % is observed which corresponds to an FRC conversion of X_{FRC} = 50.3 ± 2.38 wt % as determined by liquid-phase analysis. By using eq 5, the mass fraction of formed humin is calculated from the other species' mass fractions in Table 1 and results in w_{humin} = 1.8 ± 0.98 wt % which translates into a humin yield of Y_{humin} = 15.2 ± 8.12 mol %. The sulfuric acid mass fraction of $w_{sulfuric\ acid}$ = 6.1 ± 0.07 wt % lies above the initial value of 5 wt % at the start of the experiment. The deviation can be partially explained by the formation of solid humin material causing a decrease in the overall liquid-phase mass, which in turn results in increasing sulfuric acid fraction. Moreover, the broad pure component hard model of sulfuric acid overlaps with several other species' pure component hard models in the overall spectral mixture hard model [cf. Figure S2(F) in the Supporting Information] which can contribute to the overestimated but constant acid concentration observed in all experiments.

Figure 2 depicts the results from FESEM analysis of a humin deposit fragment from the wall of the centrifugal tube. All of the material is solid at the time of analysis. The surface of the fragment appears uniform, as visible in Figure 2A, and is covered by up to two layers of small, partially coalesced

https://doi.org/10.1021/acsomega.3c06103
ACS Omega 2024, 9, 6432−6441

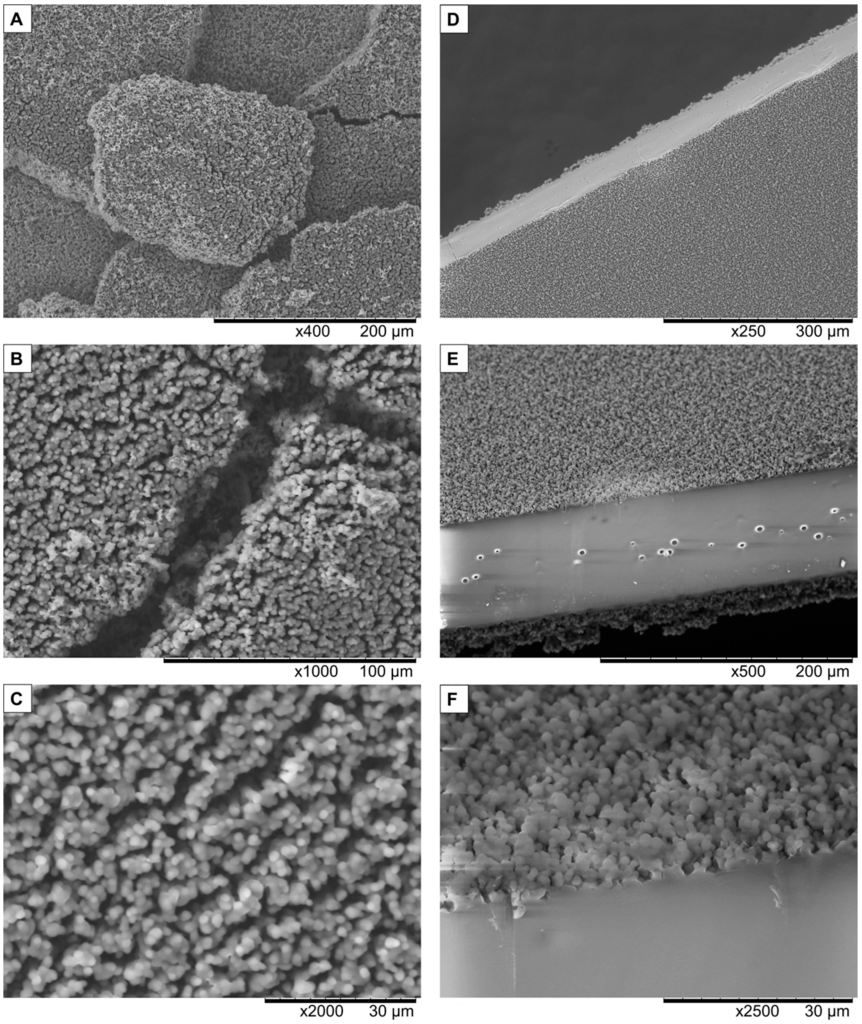

Figure 3. SEM images of humin deposits from the wall of the centrifugal tube at different magnifications for the reaction of 20 wt % FRC in an aqueous solution of 5 wt % sulfuric acid at 90 °C. (A−C) The experiment at an RCF of 4790 for 3 h yields almost monodisperse humin spheres that are partially interconnected forming a foam-like structure. (D−F) The experiment at an RCF of 13,304 for 6 h yields a thin, almost monodisperse layer of humin spheres covering a homogeneous humin bulk phase.

microspheres with a very narrow diameter range between 0.9 and 1.9 μm at an average diameter of 1.3 ± 0.3 μm, as summarized in Table 3. Figure 2B clearly shows that the microspheres cover a continuous phase with 80−90 μm thickness. The close-ups in Figure 2C,D shows the merging of the humin microspheres into the continuous phase. This indicates that humins are liquid droplets upon formation and that the repulsive forces of the humin droplets can be overcome by the application of a strong gravitational field, forcing the humin droplets to coalesce. Figure S7 in the Supporting Information shows the preparation and corresponding SEM images. Together with Figure 2C,D, it is clearly observed at several positions in the high-resolution images that humin microspheres first stick together, forming a thin layer, and ultimately merge in the continuous layer of humin deposits. These observations show that humin spheres are highly viscous droplets instead of solid particles upon formation at process conditions and ultimately coalesce to form the often-observed macroscopic particles or deposits.

Decreasing the reaction time to 3 h and the RCF to 4790 leads to an FRC mass fraction of w_{FRC} = 15.3 ± 0.50 wt % which is equivalent to an FRC conversion of X_{FRC} = 23.8 ± 2.54 wt % as determined by liquid-phase analysis (cf. Tables 1 and 2). Similar results in terms of species mass fractions, FRC conversion, and species yields are obtained for a centrifugation experiment of 3 h at an RCF of 13,304, indicating that the applied gravitational field has no influence on the liquid-phase reaction kinetics that could be measured with the employed analytical techniques and associated accuracies (cf. Tables 1 and 2).

At a reaction time of 3 h and an RCF of 4790, a humin mass fraction of w_{humin} = 0.7 ± 0.16 wt % is determined with eq 5. This corresponds to a humin yield of Y_{humin} = 6.0 ± 1.31 mol %. Compared to the results for the reaction of 6 h at an RCF of 13,304, the reaction for 3 h at an RCF of 4790 provides almost half the humin mass fraction and humin yield, which fits the expectations based on previous reaction kinetics publications, the present accuracies of the analytics, and the error propagation in the mass balance equation.[12,13,19,37,38] However, compared to the reaction at an RCF of 13,304 for 6 h, the experiment at an RCF of 4790 for 3 h delivers a very different humin phase appearance. After sample preparation (cf. Figure S6 for further details) and SEM analysis, images of the resulting humin residues (A−C) are compared against the results for an RCF of 13,304 and 6 h reaction time (D−F) in Figure 3. Similar to the experiment at high RCF, small

https://doi.org/10.1021/acsomega.3c06103
ACS Omega 2024, 9, 6432−6441

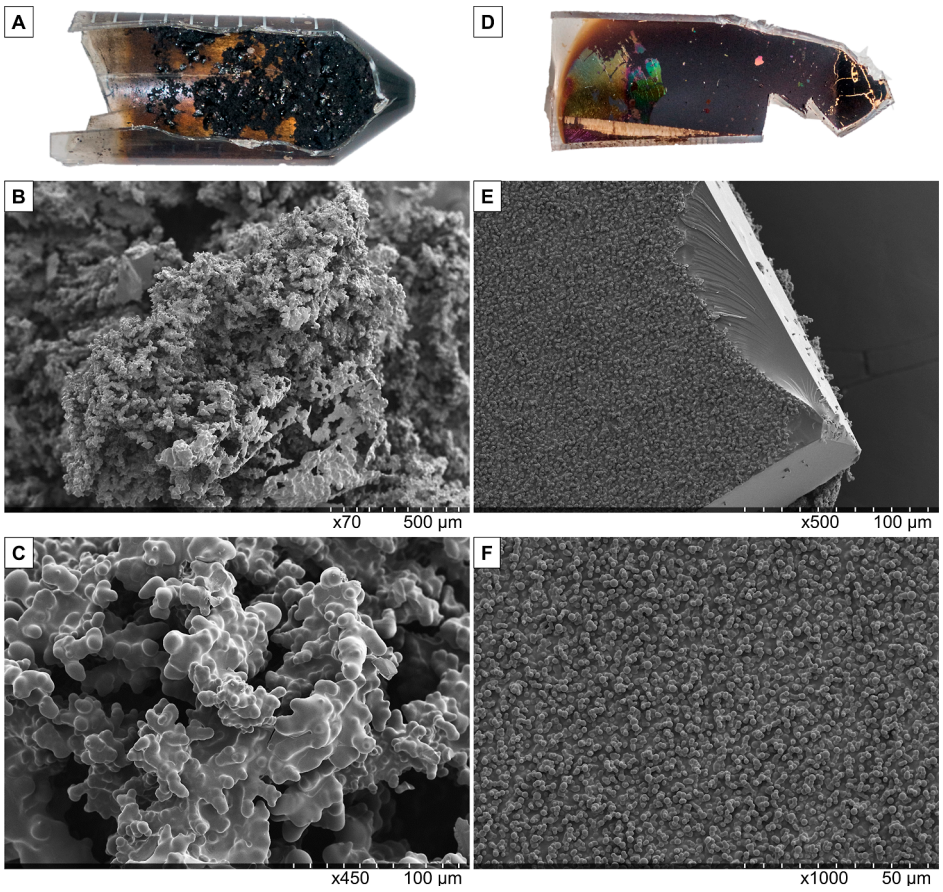

Figure 4. Cut into a centrifugal tube with humin deposits and corresponding FESEM images at different magnifications for the reaction of 20 wt % FRC in an aqueous solution of 5 wt % sulfuric acid at 90 °C. (A−C) Experiment without centrifugation (RCF = 1) and without stirring for a reaction time of 6 h, X_{FRC} = 65.5 wt %, and Y_{humin} = 15.3 mol %. (D) Centrifugal tube fragment from reaction at an RCF of 4790 for 3 h (macroscopically comparable to an RCF of 13,304 for 6 h). (E, F) Experiment with centrifugation at an RCF of 13,304 for 6 h.

microspheres of 1.1−3.6 μm at an average diameter of 2.3 ± 0.6 μm (cf. Table 3) are observed at lower RCF. However, they do not form a continuous phase but rather a foam-like structure of partially coalesced spheres (Figure 3A). The ruptures in the humin deposit layer in Figure 3B allow for insights into the layer structure and reveal a uniform, foam-like orientation throughout the whole observable layer thickness.

Executing the reaction at an RCF of 1 for 6 h in a heating block without stirring and not in a centrifuge results in an FRC mass fraction of w_{FRC} = 6.8 ± 0.86 wt % which is equivalent to an FRC conversion of X_{FRC} = 66.1 ± 4.35 wt %. The formed humin accounts for w_{humin} = 1.9 ± 0.26 wt % and Y_{humin} = 16.6 ± 2.18 mol % (cf. Tables 1 and 2). The differences compared to the reaction at an RCF of 13,304 for 6 h are assumed to arise from a faster heat transfer in the heating block setup compared to the centrifuge experiments. Consequently, the reaction temperature is reached slightly earlier, and the reaction proceeds effectively longer, causing higher values for FRC conversion coupled with increased product mass fractions and yields of small product molecules. The reaction conditions of RCF = 1 and 6 h reaction time lead to a random orientation of the humin deposits as shown in Figure 4A which is in strong contrast to the continuous humin layer obtained from centrifuge experiments (Figure 4D). FESEM images of the humin formed in the centrifugal tube confirm the randomly oriented and interconnected, larger structures with a polydisperse diameter range of 2.6−14.0 μm at an average diameter of 6.7 ± 2.6 μm (cf. Table 3) for the reaction at an RCF of 1 in Figure 4B,C, whereas the continuous humin layer with almost monodisperse spheres is displayed for the reaction at an RCF of 13,304 for 6 h in Figure 4E,F.

Comparing the SEM and FESEM images from this work in Figures 2−4 with images published in the literature shows some similarities but also clear differences that are discussed in the following. Several studies report the influence of electrolyte components such as sulfates leading to irregular, increased size of humin spheres upon longer reaction times.[3,4,21,27] According to these studies, this effect can be attributed to a reduced Debye length with subsequently reduced repulsive forces, enabling the coalescence of humin spheres. Similar effects can be clearly observed for our experiments, especially at an RCF of 1 as 5 wt % of sulfuric acid catalyst is employed. Although hydrothermal carbonization (HTC) of sugars or 5-HMF to hydrochar is carried out without sulfuric acid and at a much higher temperature of 180−240 °C, it usually results in nearly perfectly sphere-shaped humins with sphere sizes from several tens of nanometers up to 10 μm,[6,23,24] which matches ours in general. We suggest that the tight distribution of humin spheres in our experiment is due to the defined separation by centrifugation.

The most significant difference and quintessence of the images presented in our study are the formation of a thick continuous humin layer at a high RCF of 13,304 with only a few humin spheres partially coalescing on top of the layer that

https://doi.org/10.1021/acsomega.3c06103
ACS Omega 2024, 9, 6432−6441

was not reported in the literature before. These findings consolidate our assumption that humin spheres can be forced into coalescence, which provides further evidence for the viscous droplet-like behavior of humins at reaction conditions. The ubiquitous reported deposits in chemical apparatuses thus likely stem from coalesced droplets. The chemical structure of the formed humin material in the liquid state would be of high interest, but the liquid state of the humin material could not be preserved in the present study. Detailed analysis of the solid-state humins is reported elsewhere for similar conditions.[2,4,5,8] The results in Figure 3 show that our presented centrifugation-based method does not only allow for in situ separation of humin material (compare, e.g., Figures S6 and S9 in the Supporting Information: centrifugal tubes with a clear liquid phase separated from humin deposit) from the continuous liquid phase during the reaction but can also be tailored by adjustment of the RCF in addition to the usual reaction parameters such as temperature, residence time, and concentration, to control and obtain a different humin material morphology (i.e., porous or homogeneous). Consequently, this opens a new window to enable technical process designs for continuous formation and in situ humin separation that are selective for humin sizes which could be interesting for the utilization of humins as materials.

4. CONCLUSIONS

The literature on humin formation often reports the phenomenon of small regular humin spheres as the reaction product of humin chemistry. They are observed on surfaces, as residual raw materials, or as individual particles. Sometimes larger particles or even deposits have been reported, but the mesoscale mechanism of formation and deposition remained unclear because the reaction conditions do not allow direct observation. In this work, we present a method for humin formation from 20 wt % FRC at 90 °C in 5 wt % sulfuric acid integrated with separation based on systematic centrifugation experiments. The method enables in situ separation of the humin material and can be tailored by adjustment of the RCF to control the obtained humin morphology. The analysis by MIR and ^{1}H NMR spectroscopy coupled with chemometric models, based on spectral indirect hard modeling, allows for the calculation of the formed humin content as well as FRC conversion and product yields. The presented findings give evidence that humin spheres form as highly viscous droplets from the homogeneous reaction mixture as products that are immiscible in the aqueous phase. With a small difference in density, these droplets form continuously from the liquid reaction volume. A high RCF = 13,304 results in nearly monodisperse humin spheres that coalesce into a thick homogeneous layer, while a lower RCF = 4790 results in a porous structure with separate or partially merged humin spheres. At an RCF = 1, spherical structures are almost lost and randomly oriented, and interconnected large-scale structures with a high degree of polydispersity are observed. The liquid nature of the humin phase at process conditions is witnessed by the observation of different layers that form during the course of the experiment: (i) individual droplets that stick together and form a layer of nearly monodisperse spheres and (ii) a continuous layer of former humin droplets that form the deposits. While the monodisperse nature of individual droplets indicates a bulk formation of insoluble droplets, the formation of a sticky, continuous layer explains the deposits observed often under high shear conditions. The result is in line with the ubiquitous observation of small monodisperse spheres in a multitude of acidic processes with carbohydrates or biomass as feedstock. Furthermore, the observation of droplet breakup under shear stress explains the common issues with deposits in technical systems and offers a knowledge-based way to prevent such deposits by hydraulic or solvent design.

■ ASSOCIATED CONTENT

Supporting Information

The Supporting Information is available free of charge at https://pubs.acs.org/doi/10.1021/acsomega.3c06103.

Details on construction, calibration, and validation of MIR and ^{1}H NMR chemometric spectral mixture hard models; details on figures of merit for chemometric model assessment; photos of solid sample preparation; SEM and FESEM images of humin deposits; details and explanations on mass balance calculation; and pictures of solid and liquid samples from centrifugation experiments (PDF)

■ AUTHOR INFORMATION

Corresponding Author

Jörn Viell − *Process Systems Engineering, Aachener Verfahrenstechnik, RWTH Aachen University, 52074 Aachen, Germany;* orcid.org/0000-0003-0587-6151; Phone: +49 (0)241 80 97010; Email: joern.viell@avt.rwth-aachen.de; Fax: +49 (0)241 80 92326

Author

Alexander Walter Wilhelm Echtermeyer − *Process Systems Engineering, Aachener Verfahrenstechnik, RWTH Aachen University, 52074 Aachen, Germany;* orcid.org/0000-0002-9382-2227

Complete contact information is available at: https://pubs.acs.org/10.1021/acsomega.3c06103

Author Contributions

A.W.W.E.: Conceptualization and execution of experiments; construction and application of chemometric methods; SEM and FESEM analysis; discussion and analysis of measurement results; preparation and writing of the manuscript; review and editing of the manuscript. **J.V.**: Scientific support, guidance, and discussion on method and results; formulation of hypothesis; advice on structure and presentation of this work; reviewing and editing the manuscript.

Notes

The authors declare no competing financial interest.

Portions of the present work are part of the Ph.D. dissertation of the first author (A.W.W.E.): "Echtermeyer, Alexander Walter Wilhelm, Inline spectroscopy with model-based spectra evaluation for biorefinery unit operations. Chapter 5.3: Analysis of humin side product formation and deposition, Ph.D. Dissertation, RWTH Aachen University, Aachen, Germany, 2022. DOI: 10.18154/RWTH-2022-09155" that is publicly available as a PDF at https://publications.rwth-aachen.de/record/853915.[39]

■ ACKNOWLEDGMENTS

A.W.W.E. and J.V. gratefully acknowledge the financial support of the projects ContiHighSolid (031B0679) and DeMoBio (031B1135B) by the Federal Ministry of Education and Research (BMBF) and the project supervision by the project

management organization Projektträger Jülich (PtJ). Moreover, the authors thank Nina Stein, Emna Aidi, Helene Keuthen, Lena Müller, and Michelle Freyer for valuable help during the experiments as well as Karin Faensen for FESEM support. Special thanks are given to Prof. Alexander Mitsos for advice and guidance.

REFERENCES

(1) Kang, S.; Fu, J.; Zhang, G. From lignocellulosic biomass to levulinic acid: A review on acid-catalyzed hydrolysis. *Renewable Sustainable Energy Rev.* **2018**, *94*, 340−362.
(2) Sumerskii, I.; Krutov, S.; Zarubin, M. Y. Humin-like substances formed under the conditions of industrial hydrolysis of wood. *Russ. J. Appl. Chem.* **2010**, *83*, 320−327.
(3) Patil, S. K.; Lund, C. R. Formation and growth of humins via aldol addition and condensation during acid-catalyzed conversion of 5-hydroxymethylfurfural. *Energy Fuels* **2011**, *25*, 4745−4755.
(4) Patil, S. K.; Heltzel, J.; Lund, C. R. Comparison of structural features of humins formed catalytically from glucose, fructose, and 5-hydroxymethylfurfuraldehyde. *Energy Fuels* **2012**, *26*, 5281−5293.
(5) van Zandvoort, I.; Wang, Y.; Rasrendra, C. B.; van Eck, E. R. H.; Bruijnincx, P. C.; Heeres, H. J.; Weckhuysen, B. M. Formation, molecular structure, and morphology of humins in biomass conversion: Influence of feedstock and processing conditions. *ChemSusChem* **2013**, *6*, 1745−1758.
(6) Tsilomelekis, G.; Orella, M. J.; Lin, Z.; Cheng, Z.; Zheng, W.; Nikolakis, V.; Vlachos, D. G. Molecular structure, morphology and growth mechanisms and rates of 5-hydroxymethyl furfural (HMF) derived humins. *Green Chem.* **2016**, *18*, 1983−1993.
(7) Shi, N.; Liu, Q.; Cen, H.; Ju, R.; He, X.; Ma, L. Formation of humins during degradation of carbohydrates and furfural derivatives in various solvents. *Biomass Convers. Biorefin.* **2020**, *10*, 277−287.
(8) Cheng, Z.; Everhart, J. L.; Tsilomelekis, G.; Nikolakis, V.; Saha, B.; Vlachos, D. G. Structural analysis of humins formed in the Brønsted acid catalyzed dehydration of fructose. *Green Chem.* **2018**, *20*, 997−1006.
(9) Echtermeyer, A.; Mitsos, A.; Viell, J. Humin formation and deposition during acid-catalyzed biomass conversion. *Chem. Ing. Tech.* **2020**, *92*, 1290.
(10) Girisuta, B.; Janssen, L.; Heeres, H. A kinetic study on the decomposition of 5-hydroxymethylfurfural into levulinic acid. *Green Chem.* **2006**, *8*, 701−709.
(11) Swift, T. D.; Bagia, C.; Choudhary, V.; Peklaris, G.; Nikolakis, V.; Vlachos, D. G. Correction to kinetics of homogeneous Brønsted acid catalyzed fructose dehydration and 5-hydroxymethyl furfural rehydration: A combined experimental and computational study. *ACS Catal.* **2014**, *4*, 1320.
(12) Fachri, B. A.; Abdilla, R. M.; Bovenkamp, H. H. v. d.; Rasrendra, C. B.; Heeres, H. J. Experimental and kinetic modeling studies on the sulfuric acid catalyzed conversion of D-fructose to 5-hydroxymethylfurfural and levulinic acid in water. *ACS Sustain. Chem. Eng.* **2015**, *3*, 3024−3034.
(13) Jung, D.; Körner, P.; Kruse, A. Kinetic study on the impact of acidity and acid concentration on the formation of 5-hydroxymethylfurfural (HMF), humins, and levulinic acid in the hydrothermal conversion of fructose. *Biomass Convers. Biorefin.* **2021**, *11*, 1155−1170.
(14) Jung, D.; Körner, P.; Kruse, A. Calculating the reaction order and activation energy for the hydrothermal carbonization of fructose. *Chem. Ing. Tech.* **2020**, *92*, 692−700.
(15) Girisuta, B.; Janssen, L.; Heeres, H. Kinetic study on the acid-catalyzed hydrolysis of cellulose to levulinic acid. *Ind. Eng. Chem. Res.* **2007**, *46*, 1696−1708.
(16) Dussan, K.; Girisuta, B.; Haverty, D.; Leahy, J.; Hayes, M. Kinetics of levulinic acid and furfural production from Miscanthus×giganteus. *Bioresour. Technol.* **2013**, *149*, 216−224.
(17) Jiang, Z.; Zeng, Y.; Hu, D.; Guo, R.; Yan, K.; Luque, R. Chemical transformations of 5-hydroxymethylfurfural into highly added value products: present and future. *Green Chem.* **2023**, *25*, 871−892.
(18) Hu, D.; Zhang, M.; Xu, H.; Wang, Y.; Yan, K. Recent advance on the catalytic system for efficient production of biomass-derived 5-hydroxymethylfurfural. *Renewable Sustainable Energy Rev.* **2021**, *147*, 111253.
(19) Körner, P.; Jung, D.; Kruse, A. The effect of different Brønsted acids on the hydrothermal conversion of fructose to HMF. *Green Chem.* **2018**, *20*, 2231−2241.
(20) Körner, P.; Jung, D.; Kruse, A. Influence of the pH value on the hydrothermal degradation of fructose. *ChemistryOpen* **2019**, *8*, 1121−1132.
(21) Jung, D.; Zimmermann, M.; Kruse, A. Hydrothermal carbonization of fructose: Growth mechanism and kinetic model. *ACS Sustain. Chem. Eng.* **2018**, *6*, 13877−13887.
(22) Cheng, Z.; Goulas, K. A.; Quiroz Rodriguez, N.; Saha, B.; Vlachos, D. G. Growth kinetics of humins studied via X-ray scattering. *Green Chem.* **2020**, *22*, 2301−2309.
(23) Qi, Y.; Song, B.; Qi, Y. The roles of formic acid and levulinic acid on the formation and growth of carbonaceous spheres by hydrothermal carbonization. *RSC Adv.* **2016**, *6*, 102428−102435.
(24) Qi, Y.; Zhang, M.; Qi, L.; Qi, Y. Mechanism for the formation and growth of carbonaceous spheres from sucrose by hydrothermal carbonization. *RSC Adv.* **2016**, *6*, 20814−20823.
(25) Shi, N.; Liu, Q.; Ju, R.; He, X.; Zhang, Y.; Tang, S.; Ma, L. Condensation of α-carbonyl aldehydes leads to the formation of solid humins during the hydrothermal degradation of carbohydrates. *ACS Omega* **2019**, *4*, 7330−7343.
(26) Shi, N.; Liu, Q.; He, X.; Wang, G.; Chen, N.; Peng, J.; Ma, L. Molecular structure and formation mechanism of hydrochar from hydrothermal carbonization of carbohydrates. *Energy Fuels* **2019**, *33*, 9904−9915.
(27) Jung, D.; Duman, G.; Zimmermann, M.; Kruse, A.; Yanik, J. Hydrothermal carbonization of fructose − Effect of salts and reactor stirring on the growth and formation of carbon spheres. *Biomass Convers. Biorefin.* **2021**, *13*, 6281−6297.
(28) *PEAXACT*, version 5.8; S.PACT GmbH: Aachen, Germany, 2023. https://www.s-pact.de/de/peaxact-software (accessed July 24, 2023).
(29) Alsmeyer, F.; Koß, H. J.; Marquardt, W. Indirect spectral hard modeling for the analysis of reactive and interacting mixtures. *Appl. Spectrosc.* **2004**, *58*, 975−985.
(30) Kriesten, E.; Mayer, D.; Alsmeyer, F.; Minnich, C.; Greiner, L.; Marquardt, W. Identification of unknown pure component spectra by Indirect Hard Modeling. *Chemom. Intell. Lab. Syst.* **2008**, *93*, 108−119.
(31) Kriesten, E.; Alsmeyer, F.; Bardow, A.; Marquardt, W. Fully automated Indirect Hard Modeling of mixture spectra. *Chemom. Intell. Lab. Syst.* **2008**, *91*, 181−193.
(32) Meyer-Kirschner, J. Quantitative inline polymerization monitoring with Raman spectroscopy and model-based spectral evaluation. Ph.D. Dissertation, RWTH Aachen University: Aachen, Germany, 2019 (accessed July 24, 2023) https://publications.rwth-aachen.de/record/755323.
(33) Echtermeyer, A.; Marks, C.; Mitsos, A.; Viell, J. Inline Raman spectroscopy and Indirect Hard Modeling for concentration monitoring of dissociated acid species. *Appl. Spectrosc.* **2021**, *75*, 506−519.
(34) Ebrahimi, F.; Viell, J.; Mitsos, A.; Mhamdi, A.; Brandhorst, M. In-line monitoring of hydrogen peroxide in two-phase reactions using Raman spectroscopy. *AIChE J.* **2017**, *63*, 3994−4002.
(35) Kang, S.; Yu, J. An intensified reaction technology for high levulinic acid concentration from lignocellulosic biomass. *Biomass Bioenergy* **2016**, *95*, 214−220.
(36) Modenbach, A. A.; Nokes, S. E. The use of high-solids loadings in biomass pretreatment − A review. *Biotechnol. Bioeng.* **2012**, *109*, 1430−1442.
(37) Tan-Soetedjo, J. N.; van de Bovenkamp, H. H.; Abdilla, R. M.; Rasrendra, C. B.; van Ginkel, J.; Heeres, H. J. Experimental and

https://doi.org/10.1021/acsomega.3c06103
ACS Omega 2024, 9, 6432−6441

kinetic modeling studies on the conversion of sucrose to levulinic acid and 5-hydroxymethylfurfural using sulfuric acid in water. *Ind. Eng. Chem. Res.* **2017**, *56*, 13228−13239.
(38) Aigner, M.; Roth, D.; Rußkamp, J.; Klankermayer, J.; Jupke, A. Model-based equipment design for the biphasic production of 5-hydroxymethylfurfural in a tubular reactor. *AIChE J.* **2019**, *66*, No. e16849.
(39) Echtermeyer, A. W. W. Inline spectroscopy with model-based spectra evaluation for biorefinery unit operations. Ph.D. Dissertation, RWTH Aachen University: Aachen, Germany, 2022 (accessed July 24, 2023) https://publications.rwth-aachen.de/record/853915.

https://doi.org/10.1021/acsomega.3c06103
ACS Omega 2024, 9, 6432−6441